nature portfolio

https://doi.org/10.1038/s41587-021-00866-y

Supplementary information

Monitoring deep-tissue oxygenation with a millimeter-scale ultrasonic implant

In the format provided by the authors and unedited

Supplementary Notes

Nonlinearity in the IC optical readout. The optical readout nonlinearity was characterized using a function generator that produced a variable phase-shifted signal to drive the μLED. The worst-case nonlinearity, computed using the endpoint method, was less than 0.27 LSB = ~0.12° (Supplementary Fig. 1a). The τ-based Stern-Volmer plot (Supplementary Fig. 6b) reveals the nonlinearity at the system output, mainly due to heterogeneous dispersion of silica particles in the O_2-sensing film[1].

Ultrasound (US) link power transfer efficiency. The US link power transfer efficiency is defined as the ratio of the electrical input power of the integrated circuit (IC) to the acoustic power emitted from the external transducer, which depends on the beam focusing ability of the external transducer, the frequency-dependent US attenuation in the propagation media[2], and the power conversion efficiency of the implant. The acoustic power at the transducer surface was calculated by integrating the acoustic field intensity data, obtained by a hydrophone at the focal depth, over a circular area where the intensity of the side lobes is not negligible. The power conversion efficiency of the implant, relying on the receive (acoustic-to-electrical conversion) efficiency of the piezo and the impedance matching between the piezo and the IC, is equal to the ratio of the electrical input power of the IC to the acoustic power at the implant's piezo surface; the acoustic power at the piezo surface was calculated by integrating the acoustic field intensity data from the hydrophone over the surface of the implant piezo.

Effect of US link misalignment on the system operation. Although the use of acoustic waves, instead of near-field electromagnetic waves[3], enabled to power and communicate with the mm-scale wireless O_2 sensor at great depths (≥ 5 cm), it made the system sensitive to the US link alignment between the external transceiver and the wireless O_2 sensor. Therefore, it was crucial to understanding the impact of US link misalignment on the system operation.

The misalignment sensitivity of the system was evaluated by measuring the sensor V_{rect} and the uplink bit error rate (BER). The minimum V_{rect} necessary to turn on the μLED and hence to operate the sensor was ~1.36 V. The minimum acoustic intensity required to produce 1.36 V V_{rect} was 142 mW/cm^2, ~19.7% of the FDA limit (de-rated I_{SPTA}) of 720 mW/cm^2. This ~5× acoustic intensity margin provided an ability to tolerate US link misalignment for proper sensor operation while keeping the intensity at safe levels.

Alignment measurements were performed in a water tank using a 25.4 mm-diameter transducer with a focal depth of 47.8 mm, generating acoustic pulses at 2 MHz with a fixed I_{SPTA} of 220 mW/cm^2

(Supplementary Fig. 7). When the sensor was operated on the center axis of the US beam with a zero angular offset, the system could robustly operate in a wide depth range of approximately 41-57 mm without sacrificing the BER performance; measured BERs at various depths within the operating depth range were below 10^{-5}. When the sensor, positioned on the central axis of the acoustic field at the focal depth, was scanned transversely and angularly relative to the central axis of the sensor's piezo, the system also functioned properly with a 24° angular and 0.56 mm transverse offset relative to the beam central axis, at the expense of slight BER performance degradation at different angular and/or transverse offsets.

The link misalignment measurements showed that the system operation exhibited relatively high tolerance to the depth misalignment compared to the transverse misalignment, as the -3 dB depth-of-field (DOF: ~12 mm) of the single-element focused transducer is substantially higher than its beam spot size (HPBW: ~1.2 mm) at the focal depth (Supplementary Fig. 10). In practice, a fine depth alignment could be achieved by using either an acoustic standoff pad and/or ultrasound gel or an external transducer with differing focal depths. Angular alignment within the operating angular misalignment range of ±24° could be performed by careful surgical placement of the sensor in tissue. Here operation was relatively sensitive to transverse misalignment due to the transverse beam pattern produced by the external transducer. The transverse beam spot size at the desired focal length could be increased by optimizing the geometry of the acoustic lens that was built into the transducer[4,5]. A custom-designed and -built single-element transducer with a wider spot size could be used to reduce the system sensitivity to transverse misalignment, but at the expense of reduced US link power transfer efficiency.

References

1. Carraway, E. R., Demas, J. N., DeGraff, B. A. & Bacon, J. R. Photophysics and photochemistry of oxygen sensors based on luminescent transition-metal complexes. *Anal. Chem.* **63**, 337–342 (1991).
2. Goss, S. A., Frizzell, L. A. & Dunn, F. Ultrasonic absorption and attenuation in mammalian tissues. *Ultrasound Med. Biol.* **5**, 181–186 (1979).
3. Zhang, H. *et al.* Wireless, battery-free optoelectronic systems as subdermal implants for local tissue oximetry. *Sci. Adv.* **5**, eaaw0873 (2019).
4. Sato, Y., Mizutani, K., Wakatsuki, N. & Nakamura, T. Design for an Aspherical Acoustic Fresnel Lens with Phase Continuity. *Jpn. J. Appl. Phys.* **47**, 4354–4359 (2008).
5. Sanchis, L., Yánez, A., Galindo, P. L., Pizarro, J. & Pastor, J. M. Three-dimensional acoustic lenses with axial symmetry. *Appl. Phys. Lett.* **97**, 054103 (2010).
6. Chang, T. C. *et al.* Design of Tunable Ultrasonic Receivers for Efficient Powering of Implantable Medical Devices With Reconfigurable Power Loads. *IEEE Trans. Ultrason. Ferroelectr. Freq. Control* **63**, 1554–1562 (2016).

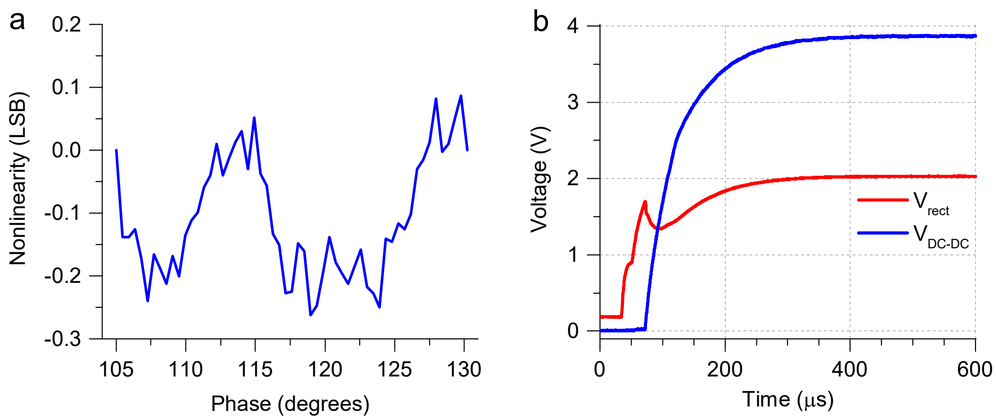

Supplementary Fig. 1 | Measured waveforms of the IC. a, Nonlinearity in the optical readout, showing that the worst-case nonlinearity was less than 0.27 LSB = ~0.12°. **b**, A rectifier voltage (V_{rect}) and a voltage doubler output ($V_{DC\text{-}DC}$) during a power-up period of ~150 µs. At steady state, the voltage conversion ratio (VCR) of the voltage doubler was 1.91.

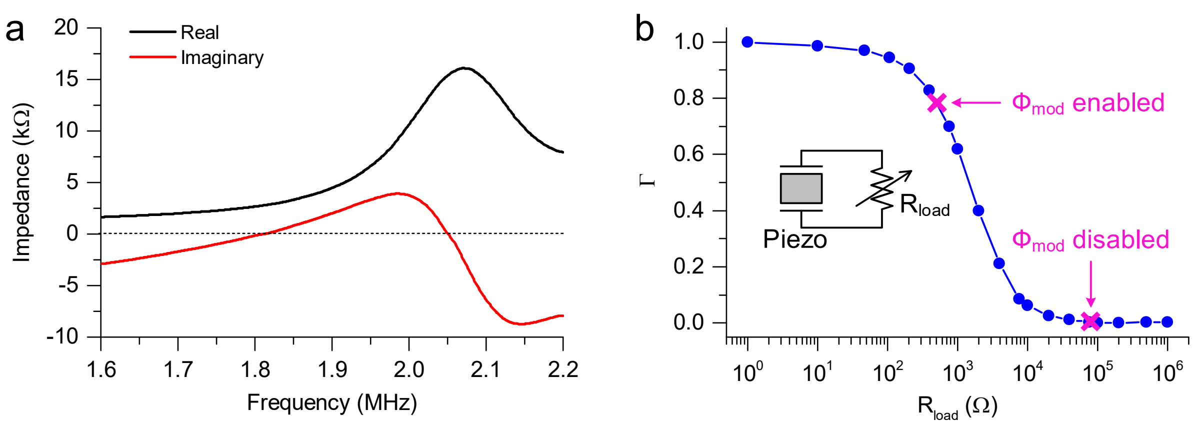

Supplementary Fig. 2 | Impedance and backscatter characterization of a 750 µm × 750 µm ×750 µm PZT piezoelectric crystal. a, Measured impedance of the ~10 µm-thick parylene-coated piezocrystal as a function of frequency in distilled water. During system operation, the piezo was driven at 2 MHz frequency that was close to its open-circuit resonance frequency of 2.05 MHz. The impedance values at 2 MHz provide a good impedance matching with the rectifier input resistance (R_{in}) of ~11.8 kΩ at the desired (2 V) rectifier output voltage, yielding an impedance matching efficiency of ~97% between the piezo and the rectifier. A capacitive matching network could be used to improve matching efficiency further[6]. **b,** Normalized acoustic reflection coefficient (Γ) of the piezocrystal versus load resistance (R_{load}), measured with ultrasound at 2 MHz. Here R_{load} simulates R_{in}.

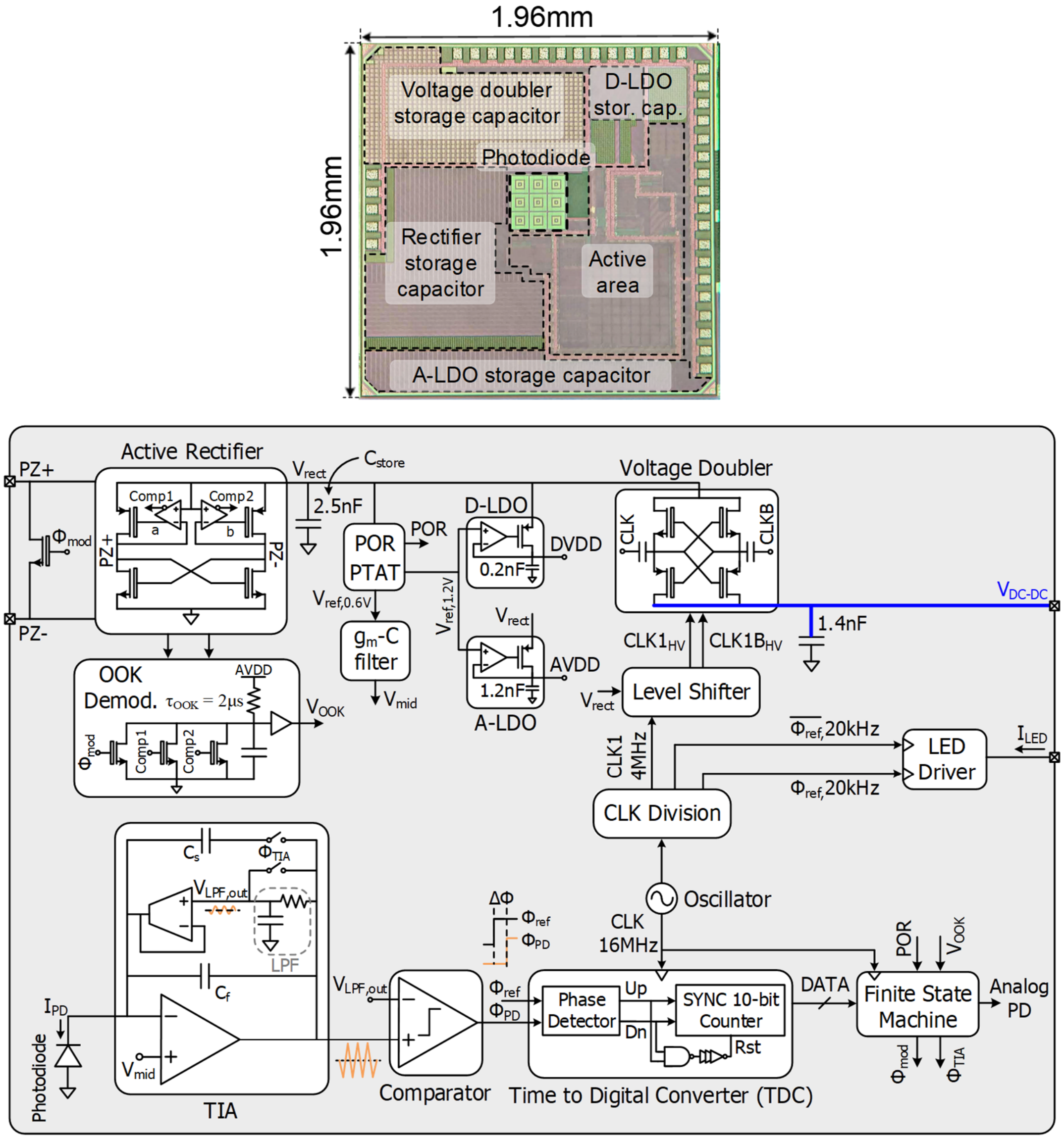

Supplementary Fig. 3 | Implant IC die micrograph (top) and a more detailed IC schematic (bottom). The IC was fabricated in a TSMC 65 nm low-power CMOS process. An analog front-end (AFE) consisted of a transimpedance amplifier (TIA), in which the DC feedback was provided using an active biasing circuit and the switches, controlled by Φ_{TIA}, were implemented to minimize the settling time after duty-cycling, and of a comparator. The rectifier comparator outputs (Comp1 and Comp2) and the modulation signal (Φ_{mod}) were used as inputs to the OOK demodulator that detected the downlink signal envelope and generated a notch. The TDC was based on a phase detector and a 10-bit synchronous counter, operating with a 16 MHz on-chip clock generated by a 5-stage current-starved ring oscillator. An LED driver was implemented using an 8-bit current digital-to-analog converter (DAC), driven by the 20 kHz complementary clock signals to avoid the rectifier voltage (V_{rect}) fluctuation. A cross-coupled voltage doubler was designed to boost V_{rect} and hence to drive the μLED.

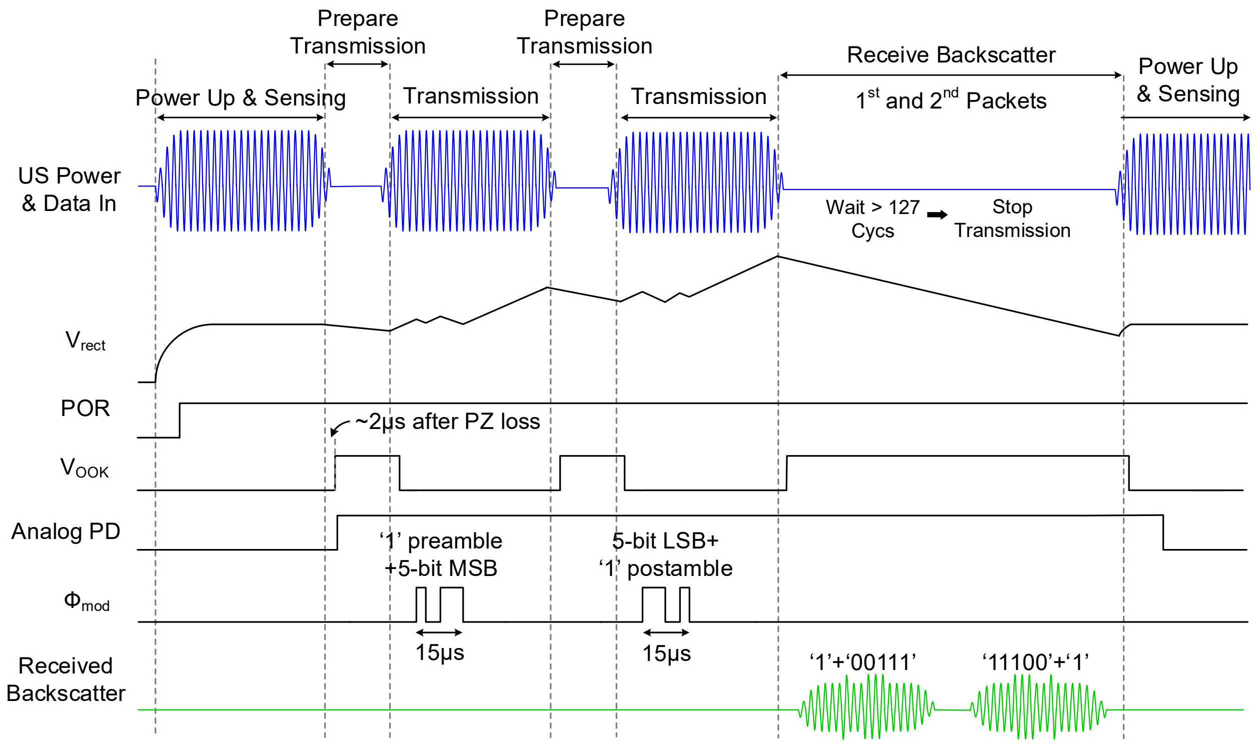

Supplementary Fig. 4 | A timing diagram for a wireless O_2 sensor implanted at a depth of greater than 5 cm. Here, the two data packets were subsequently transmitted, as in Fig. 3b, but received in a single ultrasound-free interval. Compared to the protocol in Fig. 3b, this alternative protocol reduces the time spent during uplink data transmission, which in turn allows increasing the system sampling rate.

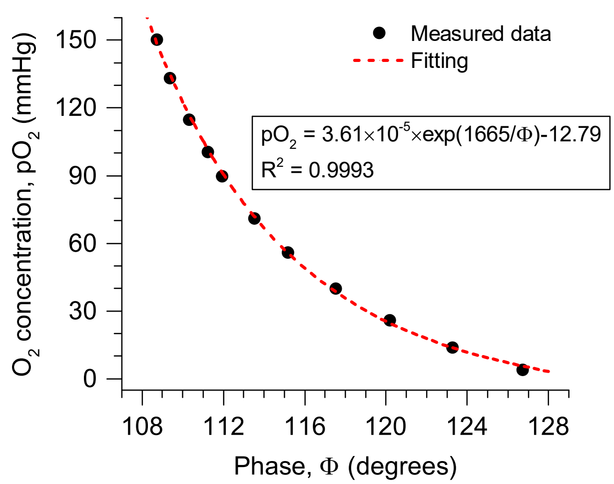

Supplementary Fig. 5 | Calibration curve of the wireless O_2 sensor. Calibration of the O_2 sensor in distilled water at 37 °C was conducted by periodically increasing the O_2 concentration of water surrounding the sensor, as shown in Supplementary Fig. 6a. The dissolved O_2 concentration was measured at each step by a commercial O_2 sensor (NEOFOX). The calibration curve was fitted by an exponential equation: pO_2 (mmHg) = $A \cdot e^{(B/\Phi)} + C$, where Φ is the sensor phase output, and A, B and C are constant coefficients obtained from the curve fitting. The exponential equation provides high accuracy with an R^2 of 0.9993. Alternative equations, such as high-order polynomial functions, could be used for calibration curve fitting.

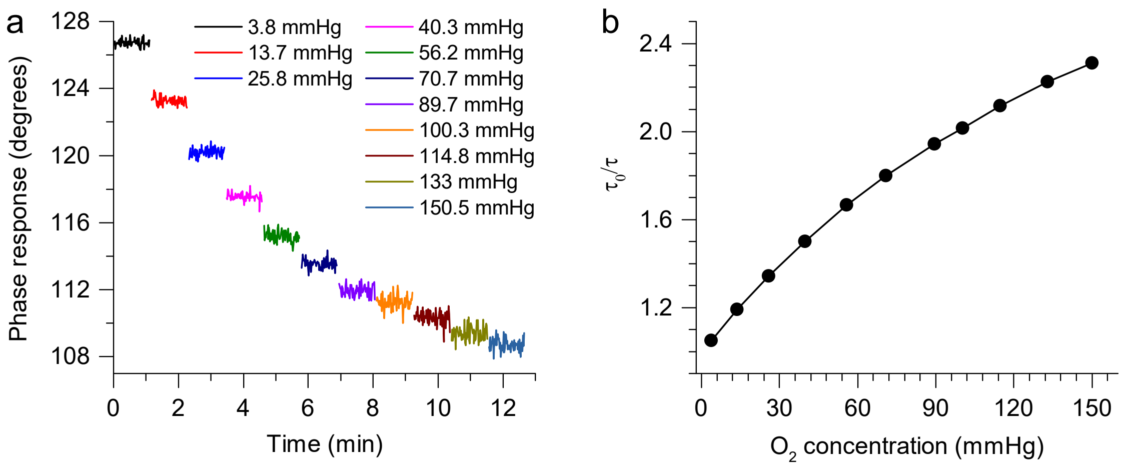

Supplementary Fig. 6 | Wireless system response to various O_2 concentrations. a, The measurement was recorded with a wireless O_2 sensor operated at 350 samples per second sampling rate and 5 cm depth during the *in vitro* characterization (see Fig. 4). **b,** Lifetime (τ)-based Stern-Volmer plot obtained using the data shown in (**a**) and the equation: $\Delta\Phi = \tan^{-1}(2\pi f_{op}\tau)$.

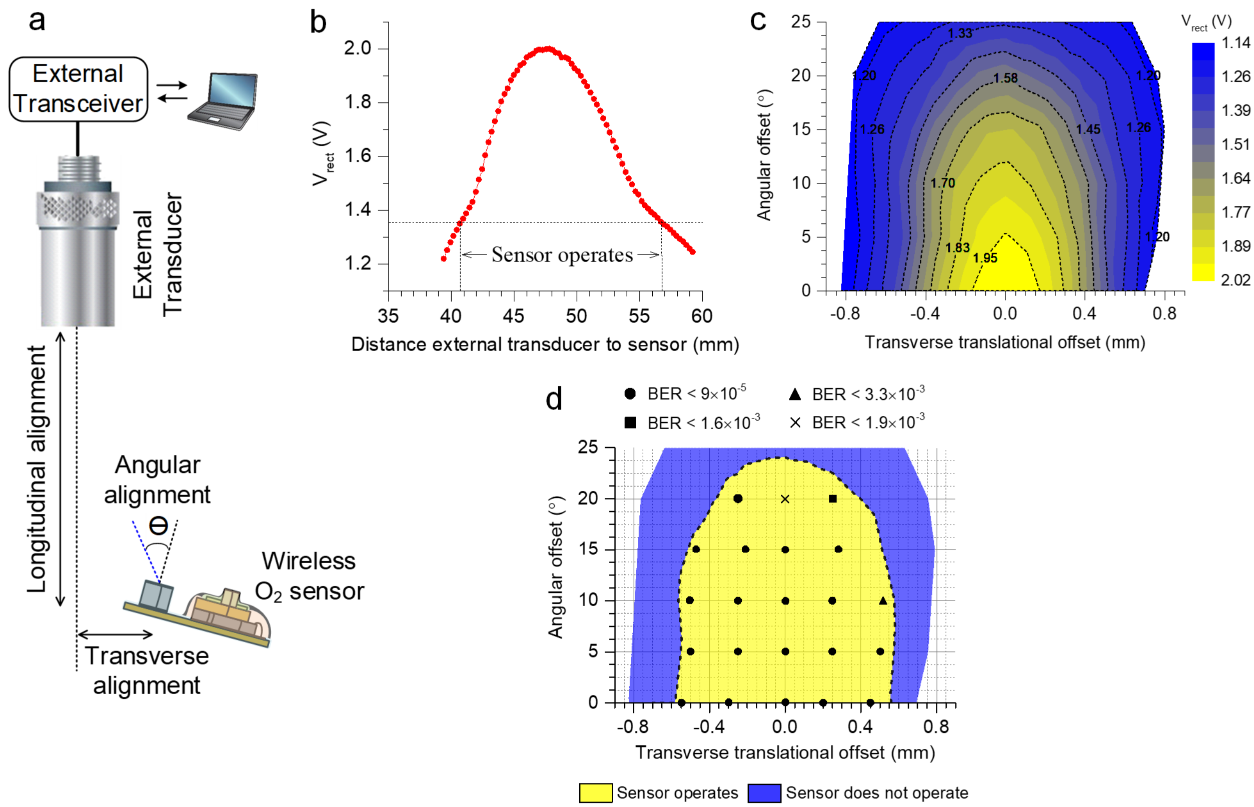

Supplementary Fig. 7 | Effect of ultrasound (US) link alignment on the system operation. a, Schematic diagram of the misalignment parameters. The measurements were performed in distilled water using a spherically focused external transducer with a diameter of 25.4 mm and a focal depth of 47.8 mm. **b-d**, A wireless O_2 sensor was operated at a fixed I_{SPTA} of 220 mW/cm^2. **b**, A wireless sensor was operated while its depth was longitudinally scanned along the central axis of the acoustic field, showing a wide operating window of 16 mm. **c**, A wireless sensor was placed aligned to the center of the focal plane at the focal depth, and its position and orientation were scanned along transverse and angular directions relative to the central axis of the sensor piezo. **d**, Color map depicted a region where the sensor operates.

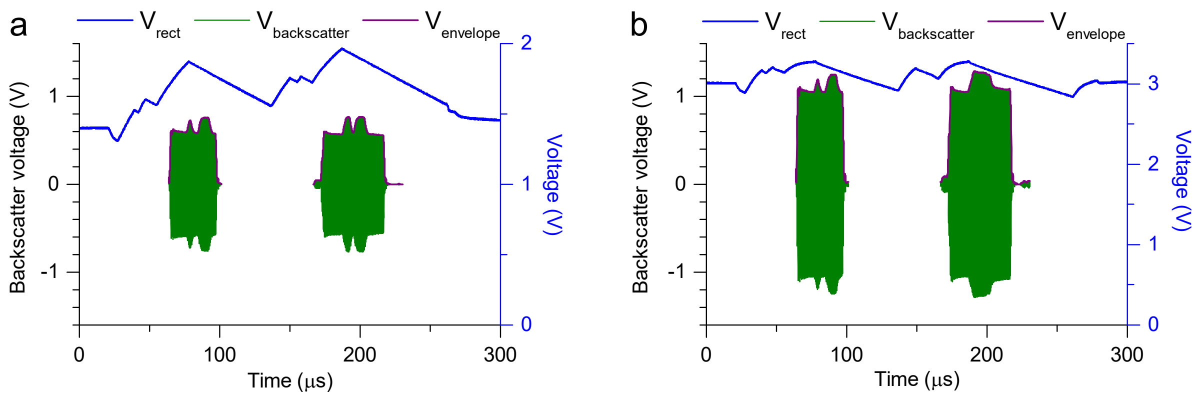

Supplementary Fig. 8 | Wireless measurement of a single O_2 sample for the sensor operated at 5 cm depth in distilled water with different acoustic intensities. The wireless O_2 sensor was operated with a 2 MHz acoustic wave with an I_{SPTA} of (**a**) 155 mW/cm^2 and (**b**) 478 mW/cm^2. The minimum rectifier output voltage (V_{rect}) required to operate the sensor was ~1.36 V (**a**). The maximum V_{rect} generated by the IC was ~3.2 V, limited by voltage limiting clamps at the rectifier input to prevent breakdown of the transistors (**b**).

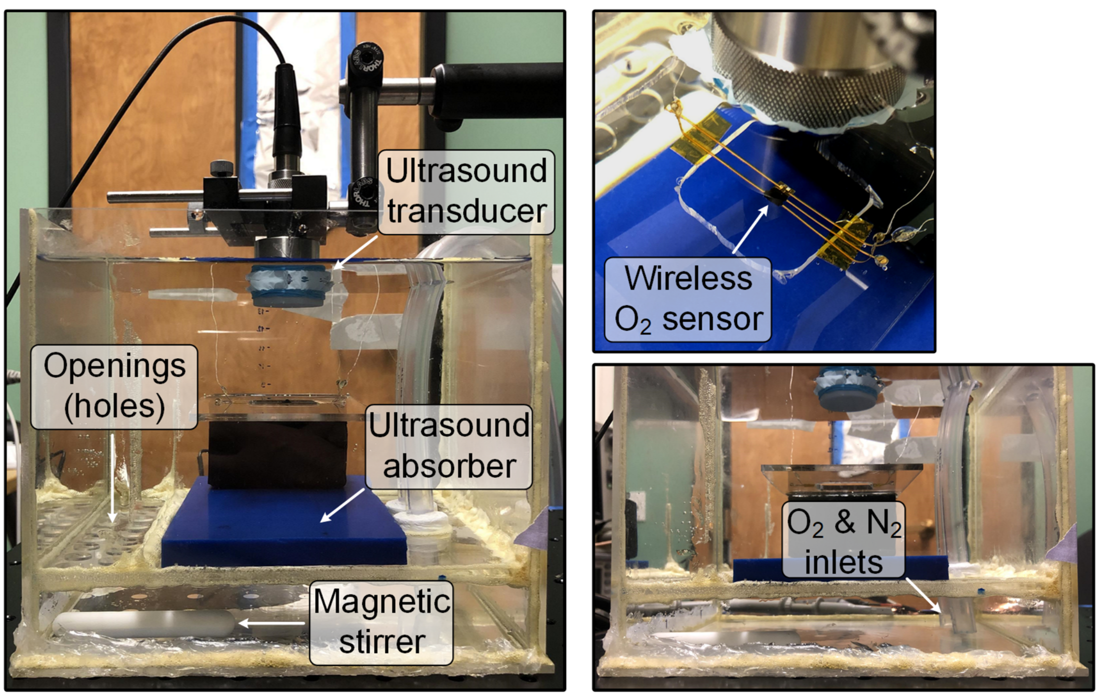

Supplementary Fig. 9 | Photograph of the custom-built water tank used for *in vitro* characterization of the wireless O_2 system. The tank consisted of two separate compartments connected through openings (holes). A magnetic stirrer in the bottom compartment facilitated the mixing of oxygen (O_2) and nitrogen (N_2), purged through the pipes, with water. An ultrasound absorber was placed to the bottom surface of the top compartment to suppress ultrasound reflections from the bottom surface during measurements.

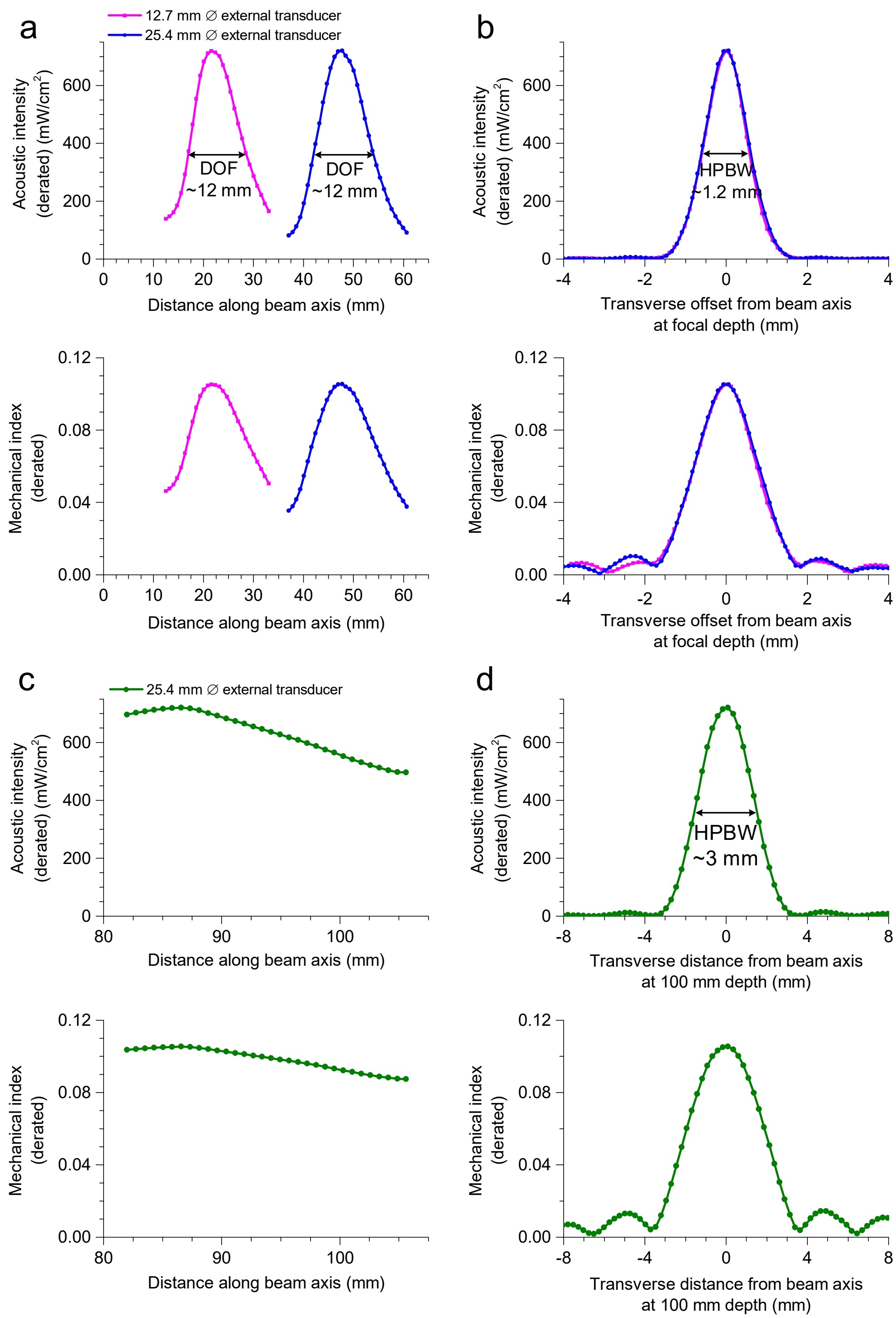

Supplementary Fig. 10 | a, b, Characterization of the external ultrasound transducers used for measurements at moderate depths ≤ 5 cm in distilled water using a hydrophone. **a,** Longitudinal beam patterns. **b,** Transverse beam patterns. **c, d,** Characterization of the external ultrasound transducer used for measurements at 10 cm depth in distilled water using a hydrophone. **c**, Longitudinal beam pattern. **d**, Transverse beam pattern.

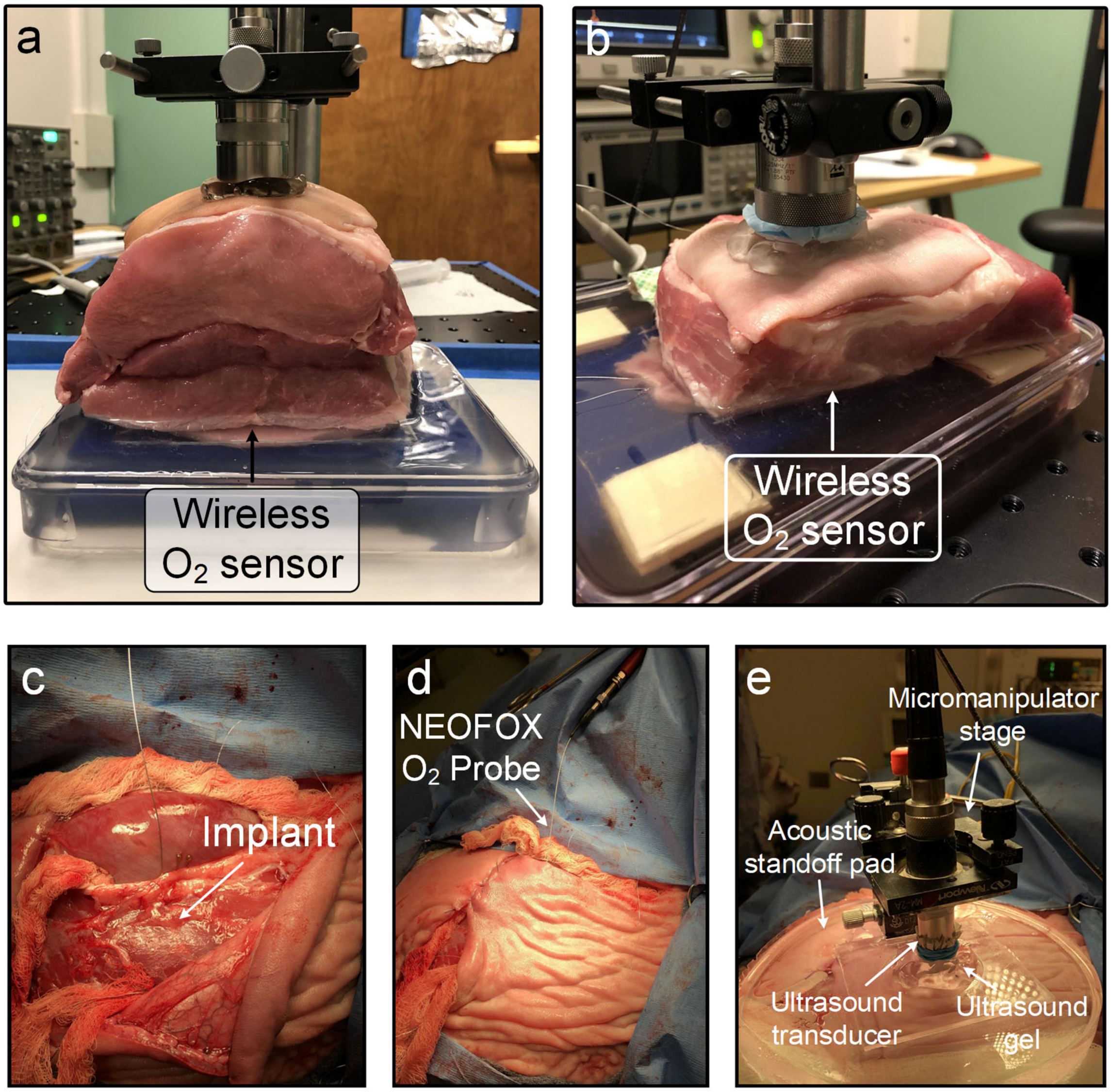

Supplementary Fig. 11 | a, An alternate photograph for Fig. 6g taken from a different perspective. **b,** An alternate photograph for Supplementary Fig. 12a taken from a different perspective. **c-e,** Photographs from animal B, showing the surgical placement of the implantable, wireless O_2 sensor in a sheep model. See Fig. 5a-d caption for descriptions.

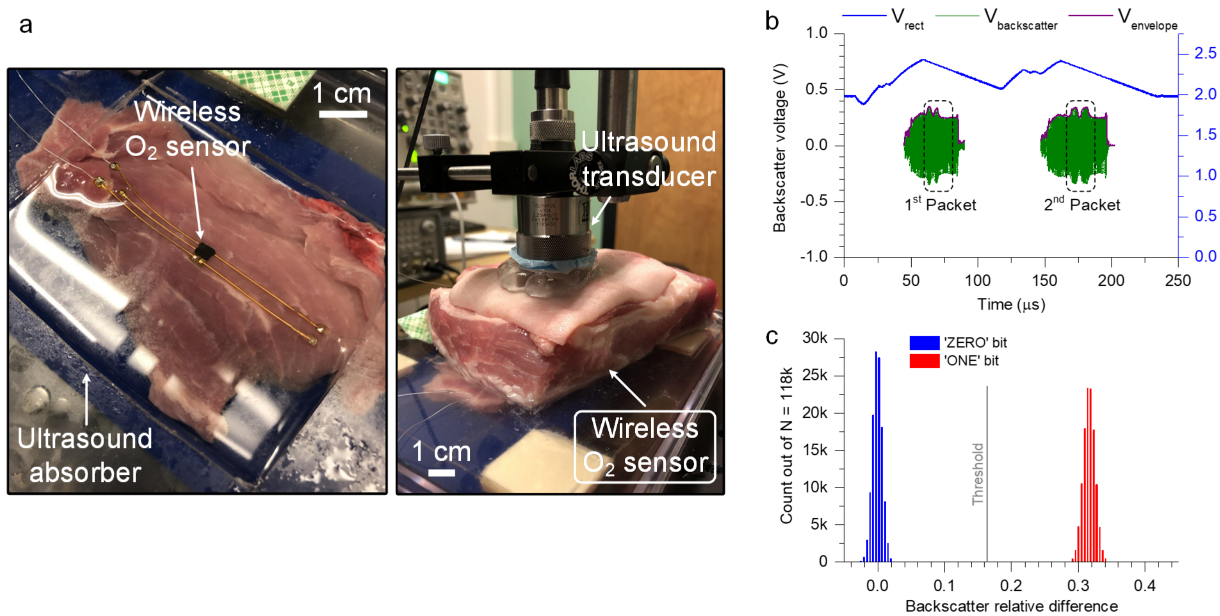

Supplementary Fig. 12 | *Ex vivo* uplink characterization of the wireless oxygen-sensing system. a, The wireless O_2 sensor was at 5 cm depth through a fresh, *ex vivo* porcine tissue specimen, in which ultrasound waves with 660 mW/cm^2 de-rated I_{SPTA}, producing an acoustic power of ~27.67 mW at the external transducer surface, propagated through approximately 2 mm ultrasound gel, 1.5 mm skin, 1 mm fat, and 45.5 mm muscle tissue. Scale bar, 1 cm. **b,** Sensor waveform and backscatter signal were captured in the wireless measurement of a single O_2 sample. **c,** Backscatter relative difference for 118k O_2 samples, showing ~32% modulation depth. The system achieved a bit error rate (BER) of < 10^{-5} and a wireless link power transfer efficiency of ~0.73%. The modulation depth measured *ex vivo* was lower than the modulation depth measured *in vitro* in distilled (DI) water (see Fig. 4d) due to a decrease in the ratio of the modulation amplitude (that is, the amplitude difference between the modulated and unmodulated backscatter signals) to the amplitude of the unmodulated backscatter signal. This ratio decrease can be attributed to the ultrasound reflections from internal tissue interfaces that interfered with the total US reflections from the sensor's piezo and the part of the sensor surface at the face of the external transducer. Note that to make a fair comparison, the alignment between the central axes of the piezo and the acoustic field was well-tuned by monitoring the rectifier voltage (V_{rect}) amplitude in this measurement and the measurement in DI water.

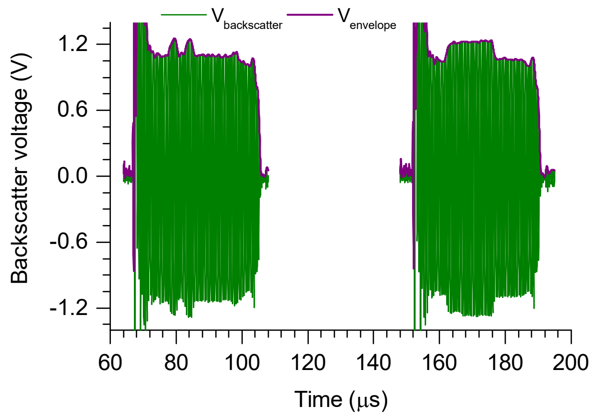

Supplementary Fig. 13 | A backscatter signal from the wireless O_2 sensor captured in an *in vivo* experiment, showing a high modulation depth of ~15%.

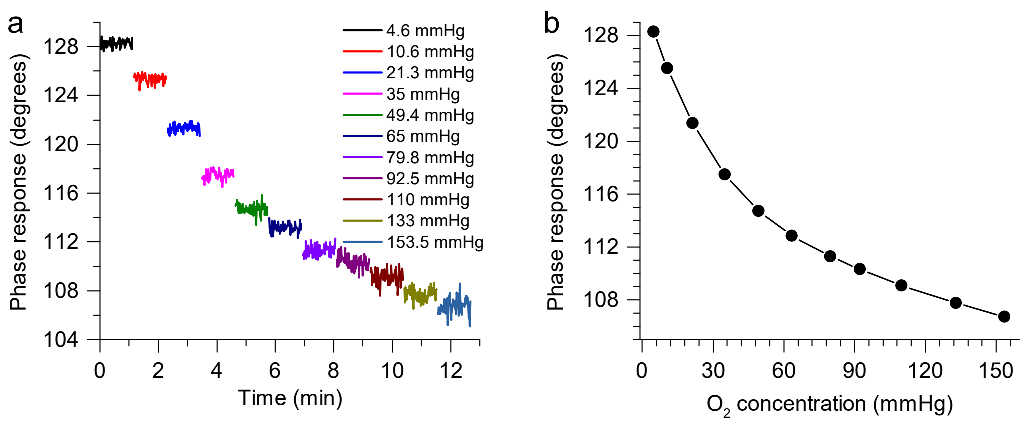

Supplementary Fig. 14 | Wireless system response to various O_2 concentrations. An additional, identical wireless O_2 sensor was also characterized in distilled water at a depth of 5 cm and a sampling rate of 350 samples per second at various O_2 concentrations. This sensor was also used for tissue O_2 monitoring. The data, shown in Fig. 5f, were collected using this sensor.